Journal of Thermal Science Vol.21, No.1 (2012) 21−31

DOI: 10.1007/s11630-012-0515-8 **Article ID: 1003-2169(2012)01-0021-11**

A Method for the Determination of Turbulence Intensity by Means of a Fast Response Pressure Probe and its Application in a LP Turbine

Davide Lengani, Berardo Paradiso, and Andreas Marn

Inst. f. Thermal Turbomachinery and Machine Dynamics, Graz University of Technology, Austria

This paper describes the measurements and the post-processing procedure adopted for the determination of the turbulence intensity in a low pressure turbine (LPT) by means of a single sensor fast response aerodynamic pressure probe. The rig was designed in cooperation with MTU Aero Engines and considerable efforts were put into the adjustment of all relevant model parameters. Blade count ratio, airfoil aspect ratio, reduced massflow, reduced speed, inlet turbulence intensity and Reynolds numbers were chosen to reproduce the full scale LP turbine. Measurements were performed adopting a phase-locked acquisition technique in order to provide the time resolved flow field downstream of the turbine rotor. The total pressure random fluctuations are obtained by selectively filtering, in the frequency domain, the deterministic unsteadiness due to the rotor blades and coherent structures. The turbulence intensity is derived from the inverse Fourier transform and the correlations between total pressure and velocity fluctuations. The determination of the turbulence intensity allows the discussion of the interaction processes between the stator and rotor for engine-representative operating conditions of the turbine.

Keywords: Turbulence, fast response aerodynamic pressure probe, low pressure turbine.

Introduction

The aerodynamic performances of turbine bladings are largely affected by the unsteadiness caused by stator-rotor interaction. In the last decades, since Binder et al. [1] and Hodson [2], many studies have been performed in turbine research facilities in order to increase the knowledge of the unsteady flow inside a turbine and improve the efficiency of highly loaded profiles. The sources of unsteadiness are numerous: secondary flows, potential flow fields and wakes, they are among the main that may be encountered in subsonic turbines. The secondary flows have a considerable effect on the whole flow field of low aspect ratio turbines (e.g. [3–5]) while for high aspect ratio ones, like the case of LPT, their effect is confined in the endwall regions (e.g. [6]). For this reason, the behaviour and generation of 2D losses have been the subject of a very large amount of studies (see for example the review by Hodson and Howell [7]). The wakes propagating from upstream are bowed and stretched as they convect through the rotor blade passages and influence considerably the evolution of the suction side boundary layer and hence cause turbulence generation and losses.

The measurement of the turbulence intensity in experimental rigs with realistic inflow conditions is needed to understand the mechanisms of loss generation and to provide realistic test cases for the validation of CFD codes. Since the beginning of the 90s, many studies on turbine rig performed turbulence measurement by means of hot-wires (e.g. [6] among many others) or Laser-Doppler Velocimeter LDV (for example Zaccaria and

Received: September 2011
Marn, Andreas Dr. techn.

Nomenclature

B_N	number of blades	Tu	turbulence intensity
BPF	blade passing frequency	v	velocity
C_{pt}	total pressure coefficient	w	relative velocity
EGV	exit guide vane	α	flow angle
EO	engine order	ρ	flow density
IGV	inlet guide vane	< >	purely periodic component
LPT	low pressure turbine	**Subscripts**	
M	Mach number	*AVE*	Circumferentially averaged properties
m_{rd}	reduced massflow	*r*	relative
n_{rd}	reduced rotational speed	*rms*	root mean square
p_t	total pressure	**Superscripts**	
PLA	phase locked average	-	time average properties
Re	Reynolds number	~	phase average properties
T	blade passing period	‘	stochastic fluctuating component

Lakshminarayana [8]). Whereas, only recently, the use of fast-response aerodynamic pressure probes (FRAPP) has been extended to turbulence measurements. Porreca et al. [9] and Persico et al. [10] have recently shown that turbulence measurements may be performed with a two-sensor and one-sensor probe, respectively. In particular, the methodology proposed by Persico et al. [10] may be adopted also for compressible flows, as performed by Paradiso et al. [11] downstream of a transonic turbine rotor, where turbulence measurements by means of a FRAPP were validated with LDV.

The work presented in this paper extends the procedure adopted in those previous papers considering the method for the determination of turbulence quantities proposed by Camp and Shin [12] and Oro et al. [13]. The raw data acquired by a miniaturized fast response aerodynamic pressure probe in a three-sensor virtual mode are transformed in the frequency domain where all the deterministic fluctuations are filtered out in order to reconstruct the unsteadiness only due to the stochastic fluctuations.

The results shown in the paper include time-resolved aerodynamic traverses performed on a research low pressure turbine. The test rig is a scaled model of the last 1 and 1/2 stage of a commercial engine and it is operated at different engine representative conditions, take-off, approach, and cruise. The paper describes the unsteady flow field downstream of the turbine rotor. The results show that, for an unshrouded rotor, the turbulence generation close to the turbine endwalls, due to the 3D flows, may not be neglected, in particular in the tip region. In fact, the flow field at the stator exit influences not only the behaviour of the rotor suction side boundary layer but also the dimension and turbulence characteristics of the secondary flows of the rotor endwalls.

Experimental facility

The Institute for Thermal Turbomachinery and Machine Dynamics (ITTM) at Graz University of Technology operates a 3 MW compressor station to supply a couple of test facilities continuously with pressurized air. In the described test facility, the maximum pressure ratio is 1.6 and the maximum massflow is 15 kg/s. In order to provide well defined and uniform inflow conditions, a de-swirler together with a perforated metal plate is mounted upstream of the test section inlet. The test turbine consists of the inlet guide vanes (IGV), the stator, the rotor and the exit guide vanes (EGV) as depicted in Fig. 1. The rig is followed by a 360 deg rotatable measurement section [14]. Finally, the air leaves the rig through the exhaust casing of the facility into the exhaust stack. A full description of the STTF-test facility is given by Moser et al. [14].

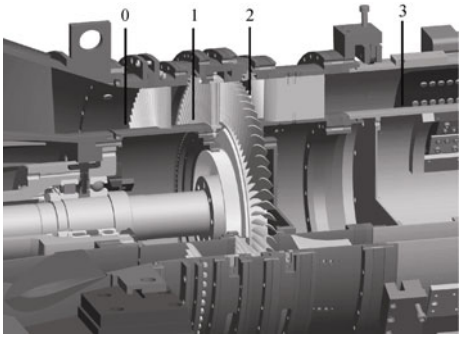

Fig. 1 Sectional drawing of the test turbine, general arrangement; results described in the paper refer to plane 2.

The aerodynamic design of the low pressure turbine was performed by MTU Aero Engines. Considerable effort was put into the adjustment of all relevant model parameters to reproduce the full scale LPT situation. The turbine diameter and the rotating speed are approximately half of those of a commercial aero engine LPT. A section of the rig is shown in Fig. 1 where 0, 1, 2, and 3 indicate the probe measurement positions. The 1 and 1/2 stage is representative of the last stage of a commercial engine with turbine exit casing. Table 1 shows the blade count and the main geometrical details of the turbine.

Operating conditions

Experiments are carried out in three different flow conditions: high Reynolds number and nominal incidence (take off), low Reynolds number and nominal incidence (cruise) and low Reynolds number and negative incidence (approach). The operating points were defined using an aero design point of the last stage of a LP turbine, derived from current LP turbine design practice using scaling along reduced speed, massflow and pressure ratio. Table 1 shows the reduced massflow, the reduced speed, and the Reynolds and Mach numbers of the operating points. The reduced mass flow and speed are referred to 288.15 K and 1013.25 mbar. The Reynolds and Mach numbers are defined with the midspan conditions at the rotor exit. Take-off and approach operating points were designed in order to maintain a full similarity with the real engine while the Mach number for the cruise operating point is not representative of the real value. Nonetheless**,** it is well known that for LP turbines, the Reynolds number is the most crucial flow parameter to be respected (see for example Hourmouziadis [15]).

Table 1 Geometry details and flow conditions.

Geometry details			
Number of blades/vanes IGV/Stator/Rotor/EGV			83/96/72/15
Stator-rotor axial gap			13 mm
Chord length (stator at midspan)			19 mm
Chord length (rotor at midspan)			25 mm
Chord length (EGV)			100 mm
Tip gap			0.8 mm
Tip gap to blade height ratio			1%
Inner diameter			155 mm
Outer diameter			235 mm
Flow parameters			
	Take-off	Cruise	Approach
Re	2.4×10^5	1.5×10^5	1.5×10^5
M_r	0.53	0.35	0.35
m_{rd}	8.97	7.0	7.0
n_{rd}	5206	3090	4070

Cylindrical high response pressure probe and measurements set up

Unsteady flow measurements were performed by means of a cylindrical single-hole fast-response aerodynamic pressure probe, operated as a virtual three sensor probe for 2D aerodynamic measurements. A miniaturized pressure sensor (Kulite XCE-062) is mounted inside at the axis of the probe head, the outer diameter of which is 1.85 mm, more details on the probe design may be found in Ref.[16].

The present paper describes the results obtained in different circumferential positions in plane 2 downstream of the rotor (marked in Fig. 1). The plane is located at 60% of the rotor axial chord downstream of the blade trailing edge. The measurement grid consists of 28 positions along the blade span and 35 positions over one EGV pitch. The probe aerodynamic accuracy was evaluated in a calibrated nozzle, resulting in an extended uncertainty equal to ±0.5% of the kinetic head for the pressure measurements and ±0.3 deg for the flow angle. Details on the transfer function of the probe are given in Ref.[16] where the probe was calibrated in a low-pressure shock tube. The probe bandwidth is up to 80 kHz, after digital compensation.

The probe measures directly the total pressure within a certain flow angle insensitivity (±10 deg in the present case). This is a typical characteristic of cylindrical pressure probes and it was verified during the calibration. Total pressure fluctuations may be then derived if the instantaneous flow angle fluctuation remains inside the insensitivity range, where the pressure measured by the probe is the instantaneous total pressure [10]. Nonetheless, downstream of a turbine rotor the flow angle may change considerably during the blade passing period and within this period, for a constant position of the probe, the flow angle may go beyond the insensitivity of the probe. This problem may be overcome by using multiple rotations of the probe and by assuming that the flow angle stochastic fluctuations at a certain phase of the rotor revolution do not exceed the flow angle insensitivity. For the present probe, rotations with a span of 20 deg are theoretically sufficient to assure the measurement of the instantaneous total pressure at any phase. However, in order to extract the flow quantities with a minimum number of rotations, a span of 15 deg between the multiple rotations has been chosen. The flow quantities are then derived from the 3 rotations with a span of 45 deg, according to the calibration coefficients.

The number of extra-rotations depends on the amplitude of the flow angle deterministic unsteadiness that was evaluated through preliminary measurements. The flow angle variations in one blade passing period stay within the probe insensitivity if the probe is aligned with the

mean flow direction for 80% of the blade span from the hub. Whereas in the tip region, since the rotor is unshrouded, the tip leakage vortex introduces large angle fluctuations as shown in Fig. 2. In the figure the 0 deg angle corresponds to the mean flow direction, and during one blade passing period the angle variations (Δα) varies from almost -20 deg. to +20 deg. By means of 9 rotations marked in the figure it is possible to measure the instantaneous total pressure p_t and determine the flow properties by means of the triplets of rotations indicated. For example for the phase corresponding to t/T = 0.4 (light grey symbols in the graph) the total pressure is read by the rotation at −15 deg and the flow properties may be derived from the triplet of rotations -60/-15/30. Similarly for the phase t/T = 0.8 and the dark grey triplet and symbols, or for t/T = 0.1 and the black marks. Each phase is then associated with a rotation of the probe in order to follow, "virtually", the time-resolved flow angle. The instantaneous pressure fluctuations are computed at the correct rotation for the corresponding phase and then the distribution of the root mean square of the total pressure fluctuation $p'_{t,rms}$ may be reconstructed for a whole revolution. The procedure to obtain $p'_{t,rms}$ and consequently the turbulence intensity inside the turbine is described in the following sections.

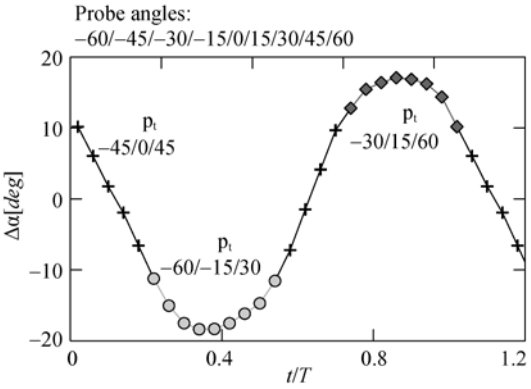

Fig. 2 Time resolved distribution of the flow angle at a fixed probe position, close to the turbine tip.

Data reduction method

Data are acquired at 500 kHz for 100 revolutions of the turbine, the total number of collected samples varies according to the turbine rotational speed. The acquisition, for any rotation of the probe, lasts around 2 seconds for the "cruise" operating point and 1 second for the "take off" one. The raw signal is digitally compensated by using the experimental transfer function. Then, the "adaptive resampling" process [17] has been applied to the signal: the sampling frequency is adaptively corrected with respect to speed variations of the turbine shaft, by means of the analysis of the shaft encoder signal. In particular, each revolution is resampled to a number of 1024 samples and the sampling frequency after this procedure may be easily computed and corresponds to 1024·BPF/B_n. The resampled data are then phase averaged and at this point the flow properties are derived. The unsteady flow quantities, measured in the absolute frame, are extended to the relative frame to enhance the comprehension of the flow structure of the rotor. The procedure adopted to derive relative quantities is performed according to what described by Gaetani et al. [18].

Determination of velocity fluctuations

A classic approach to determine the fluctuating component of a variable p is the decomposition according to the triple decomposition procedure [19]:

$$p(t) = \overline{p} + < p(t) > + p'(t) \tag{1}$$

where $<p(t)>$ is the purely periodic component associated with the rotor rotational speed and $p'(t)$ is the random fluctuation associated mainly with turbulence. The contributions of the time-mean and the purely periodic parts give the overall ensemble-averaged pressure:

$$\widetilde{p}(t) = \overline{p} + < p(t) > \tag{2}$$

Then, according to Eq. 1, the random fluctuating component of the total pressure $p'(t)$ may be computed subtracting from the instantaneous total pressure $p(t)$ the ensemble average value (t). This procedure is normally equivalent to the procedure proposed by Camp and Shin [12] and applied by other authors (e.g. [13]) that consists of the following steps:

1) The original signal is transformed into the frequency domain performing a Fourier transformation.

2) The amplitude of the periodic components related to the rotor rotational speed is digitally filtered out setting their amplitude to zero.

3) The "chopped" spectrum is transformed back into the time domain to give the turbulent signal $p'(t)$.

Furthermore, the fluctuating component $p'(t)$ is commonly referred as "unresolved unsteadiness" (see for example Suder et al. [20]) since it may contain deterministic (large scale structures) and stochastic unsteadiness. An extension of the procedure proposed by Camp and Shin [12] is to filter out the deterministic unsteadiness due to large coherent structures at frequencies non-correated to the rotational speed of the rotor. This is the case of the present test turbine, due to the low aspect ratio of the EGV there are peaks in the amplitude spectrum at frequencies non correlated to the rotational speed.

Figure 3 shows non-dimensional amplitude spectra obtained from averaging 175 measurement positions at midspan downstream of the rotor (5 radial traverse time and 35 circumferential positions). In the abscissa, a dimensionless frequency, called engine order (EO), is used. It is defined EO = 1 for the frequency of the rotational speed, with this definition, the blade passing frequency corresponds to the number of blades (72). Two different

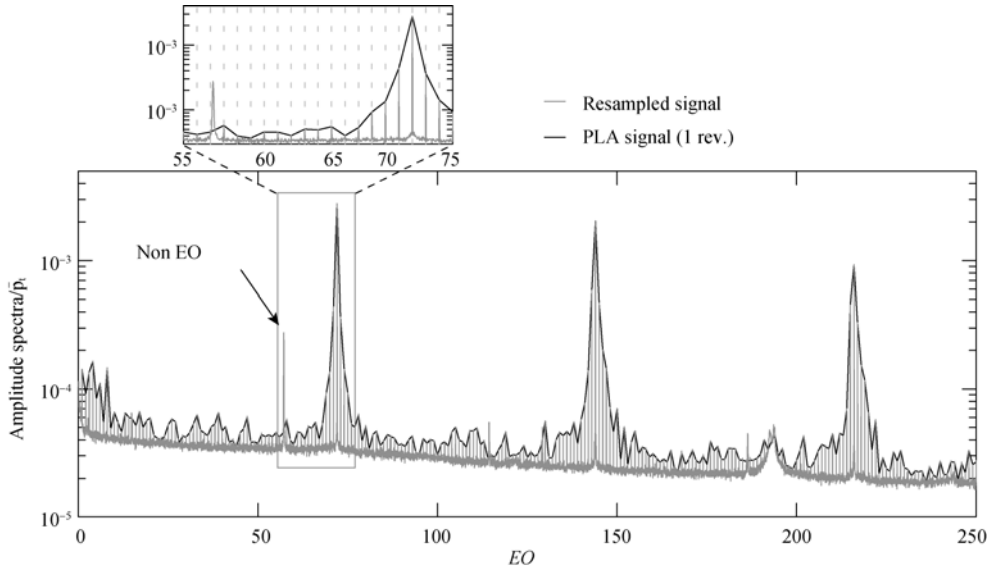

Fig. 3 Average non-dimensional amplitude spectra at rotor midspan

spectra are shown, the grey one is obtained from 64 revolutions of the original signal resampled according to the "adaptive resampling" process described before. While the spectrum in black is obtained from one revolution, namely the phase locked average over the 100 revolutions that have been acquired. Due to this kind of post processing the spectrum obtained from the resampled signal shows very clear spokes at each engine order. In fact, the frequency resolution, after resampling, is forced to be a sub-multiple of an EO. This effect may be more clearly observed in the zoom performed in the region close to the BPF and shown at the top of the graph. In addition, the average signal (black spectrum) is the envelope of the peaks at the integer engine orders.

A sharp frequency peak, non engine order, may be observed in the graph between 55 < EO < 60 (see the zoom) that is filtered out by the PLA procedure, black spectrum in the zoom. Similar peaks (non engine order) with lower amplitude may also be observed at higher frequencies. In particular, the peak at EO ≈ 57.25 corresponds to the pressure fluctuation induced by the vortex shedding frequency of the EGV and propagating upstream. The amplitude of this phenomenon is relevant even with respect to the BPF because of the very low aspect ratio of the EGV. This characteristic is also probably causing a very strong interaction between the wake and the secondary flows which would increase the amplitude of such phenomenon.

The application of the classic method to determine the fluctuation of total pressure (Eq. 1) would consider this coherent pressure fluctuation as a part of the unresolved unsteadiness. Whereas, the Camp and Shin [12] procedure may be extended filtering also the peak frequencies of this coherent structure. This last procedure may be considered as a better evaluation of the turbulence structure since it has the contributions to the unsteadiness as a result that large coherent structures are systematically removed.

The extension of the Camp and Shin [12] procedure is schematically represented in Fig. 4. One of the most critical points of their procedure is the determination of the periodic components related to the rotor structures. However, the resampling of the signal, as described before, allows the determination of sharp peaks at each EO, namely they represent all the deterministic unsteadiness correlated to the rotor rotational speed within one revolution. Hence, the filtering of each EO removes all the rotor periodic components.

Considering Fig. 4, the fluctuating part of the total pressure may be determined with the following steps:

1) The original signal is resampled and an FFT is performed over a sufficiently large block of samples in order to have a high resolution of the FFT (16/32 points between each EO).

2) The amplitude of the periodic components (integer EO) and peaks, due to large coherent structures, is digitally filtered out setting their amplitude to zero.

3) The "chopped" spectrum is transformed back into the time domain and phase locked averaged to give the root mean square of the random unsteady fluctuations.

As shown in Fig. 4 the final result is expressed in terms of fluctuations of velocity that may be obtained by considering the link between fluctuations of total pressure $p'_{t,rms}$ (measured by the FRAPP) and fluctuations of velocity as proposed by Wallace and Davis [21] and Persico et al. [10, 22]. In particular, for an isotropic compressible flow the velocity fluctuations v'_{rms} in the streamwise direction may be computed from the follow-

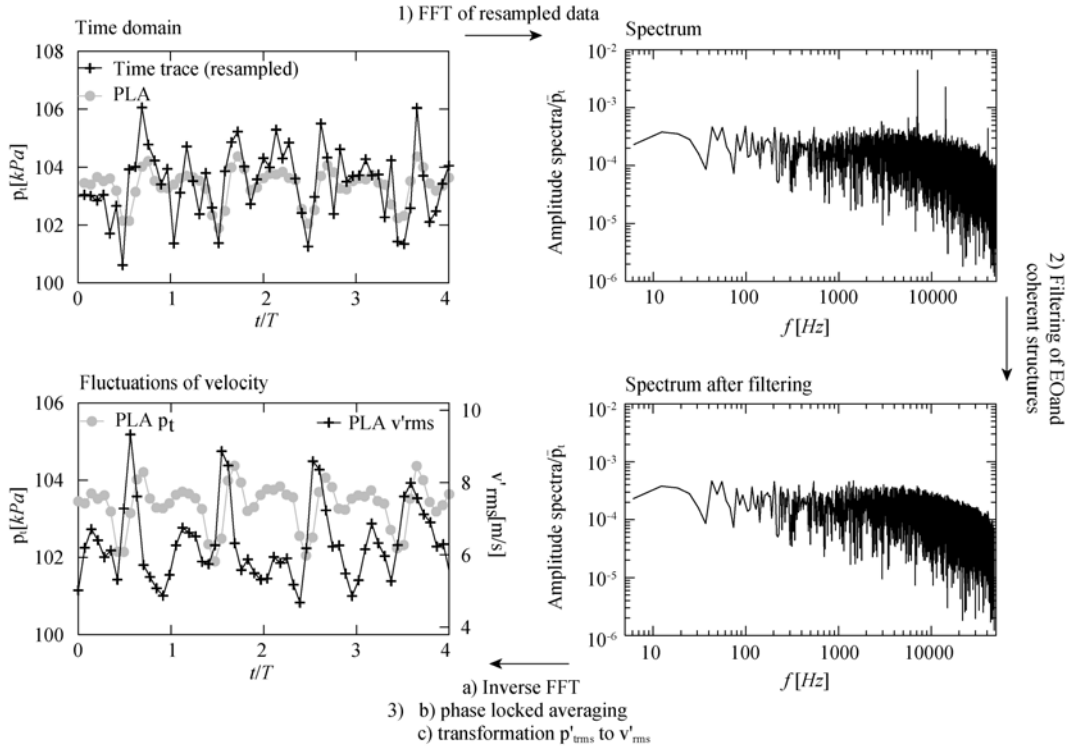

Fig. 4 Schematic representation of the post-processing procedure

ing formula [10]:

$$p'^2_{t,rms} = 0.49\rho^2(1-0.175\overline{M}^4)^2 v'^4_{rms} + \\ + \rho^2\bar{v}^2(1+0.5\overline{M}^2)^2 v'^2_{rms} \quad (3)$$

Further assumptions, see Persico et al. [22], may allow the conversion from the instantaneous pressure fluctuation to the instantaneous turbulent velocity that may be used for the computation of the integral length scale.

It has to be noted that the procedure described here may be applied not only to the fast response aerodynamic pressure probes. Aside the last point, where total pressure fluctuations are converted in velocity fluctuations, the procedure may also be applied to the measurement techniques that directly detect the velocity (e.g. hot-wires).

Results and Discussion

The time-resolved evolution of the flow downstream of the turbine rotor is discussed in this section. The results are shown in terms of an average-blade passing period since the asymmetries of the rotor were negligible. In fact, from the spectral analysis of the signal it shows that almost the whole signal energy is included at the blade-passing frequency and its harmonics. As observed from Fig. 3, the amplitude of the peaks at EO different from the BPF is much lower than the amplitude at the BPF and its harmonics. Thus the average among the 72 blade passages has been computed. Due to the large number of blade passing periods (B_n = 72) it is possible to compute an average-representative blade passing period with a larger number of samples. While there are around 14-15 samples per blade passing period in the resampled signal (computed as samples per revolution divided number of blades), the resolution of the average-representative blade passing period is equivalent to 25 points that corresponds to a temporal resolution of t/T = 0.04.

Before discussing the time resolved evolution of the flow in the three operating conditions, a time-snapshot of the flow field is discussed by analyzing Fig. 5 to provide an overview of the basic structures of the flow downstream of the rotor. A contour plot of the relative Mach number in the absolute (stationary) reference frame for the take-off operating condition is shown in the picture for one phase of the rotor. The plot is a view in the downstream direction of a sector covering one pitch of the exit guide vane and consequently 6.4 pitches of the stator vane and 4.8 rotor blade passages.

The flow features that are caused by the rotor blades, hub secondary vortex, the tip leakage vortex and the rotor wake, may be identified in Fig. 5 where their positions are marked for the experimental results. The largest velocity defects occur in the endwall regions. The tip leakage vortex, identified in the picture with the symbol TLV for one blade passage, shows considerably lower relative Mach numbers than the hub secondary vortex (HSV in picture). At the tip there is a very strong interaction be-

tween the jet-like leakage flow and the mainstream flow (e.g. [23, 24]) which generates this vortical structure with very low momentum that characterizes around 80% of the blade passages in this region (a similar result was found in Ref. [25] for an unshrouded high pressure turbine with a moderate high aspect ratio). Furthermore, as observed in many other studies (e.g. [6]) the radial pressure gradient causes fluid to migrate toward the hub. This effect may be observed in the velocity distribution inside the blade passage. The relative Mach number below midspan has larger values than above.

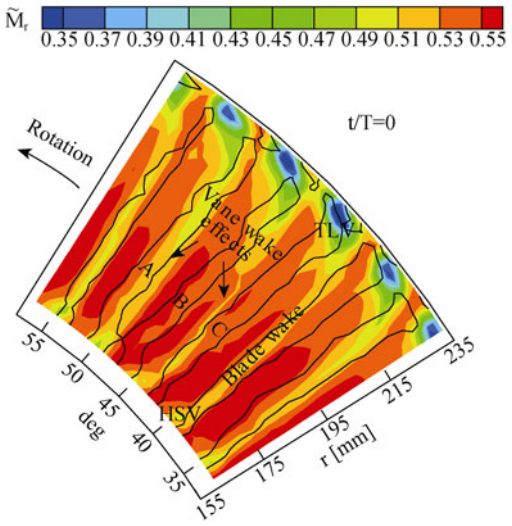

Fig. 5 Time-snapshot of the relative Mach number (take-off operating point); the dominant structures of the flow are marked over the experimental results.

Due to the high aspect ratio of the rotor blade, the region between 15% and 80% passage height is characterized by velocity defects related to the blade wakes. In particular, the flowfield at the stage exit is the result of two dimensional interaction mechanisms like vane wake blade interaction, which has been largely documented since the mid of the 80s [1, 2]. Furthermore, since the number of vanes and blades of the turbine is unequal, adjacent rotor blades face different flow structures from the stator and, then, the outlet flow of adjacent blade passages is not uniform along the circumference. These circumferential non-uniformities are marked in Fig. 5 as vane wake effects since they are due to the different interactions between vane wakes and blades. To allow the identification of the stator flow structure positions, an isocontour line of the time- averaged total pressure coefficient is superimposed on the plot of Fig. 5. This total pressure coefficient is defined as the difference between the time averaged total pressure and its circumferential average and made non dimensional:

$$\overline{C}_{pt} = \frac{\overline{p}_t - p_{t,AVE}}{0.5\rho w_{AVE}^2} \tag{4}$$

Time averaging total pressure removes the effect of rotor and thus allows the position of the vane structures to be determined as performed in Ref. [25]. In fact, the number of regions enclosed by the isocontour lines of $\overline{C}_{pt} = -0.02$ corresponds exactly to the number of the upstream stators. These regions at negative pressure coefficient are due to the stator structures. In fact, as stated by Binder et al. [26], even if the vane wakes are chopped and stretched by the rotor viscous and potential effects, leaving the rotor along avenues, the vane wakes are always fixed relative to the upstream vane position.

The rotor wake is wider in position A (marked in the plot) where it is superimposed on the region at low $\overline{C}_{pt}$. While in positions B and C, the areas at low $\overline{C}_{pt}$ are superimposed on the core flow of the rotor, and the blade wake between these two positions presents a very small width. A similar distribution may be observed in the hub secondary flows while the opposite trend is shown in the tip leakage vortex. In position A, its velocity defect is the lowest among the others at different circumferential positions. All these structures, the blade wakes and secondary flows, depend on the relative position of the rotor with respect to the vane position, and they are changing as the rotor moves, the complex unsteady interaction is discussed in details by Lengani et al. [27].

To compare the unsteady evolution of the flow at different flow conditions, results are presented in Figs. 6a and 6b as contour plots of the relative Mach number and turbulence intensity, for take-off, cruise, and approach (shown from top to bottom of the figure). These plots represent the temporal evolution of the flow along the span of the blade for two different circumferential positions: maximum and minimum of $\overline{C}_{pt}$. Data are post-processed in order to show the rotor wake at a fixed temporal position, $t/T \approx 0.55$. The suction side may be identified on the left of the wake position, and the pressure side on the right. It has to be noted that two identical blade passing periods are reproduced on each graph just to make it more readable. The turbulence intensity is obtained dividing the phase locked averaged velocity fluctuations $\tilde{v}'_{rms}$ by the phase locked averaged modulus of the velocity.

The flow features identified in Fig. 5 may be clearly observed also in Fig. 6a. The largest velocity defect may be observed in the tip leakage vortex region at the three operating points. As observed in Fig. 5, this structure is slightly dependent on the circumferential position. For the position at maximum $\overline{C}_{pt}$ the velocity defect involves a larger portion of the blade passing period than for the position at minimum $\overline{C}_{pt}$, for take off and cruise. For approach, because of the incidence variation, the trend is different. The penetration of this structure on the blade span is larger for all the operating points at the minimum $\overline{C}_{pt}$. This is the result of a very complex in-

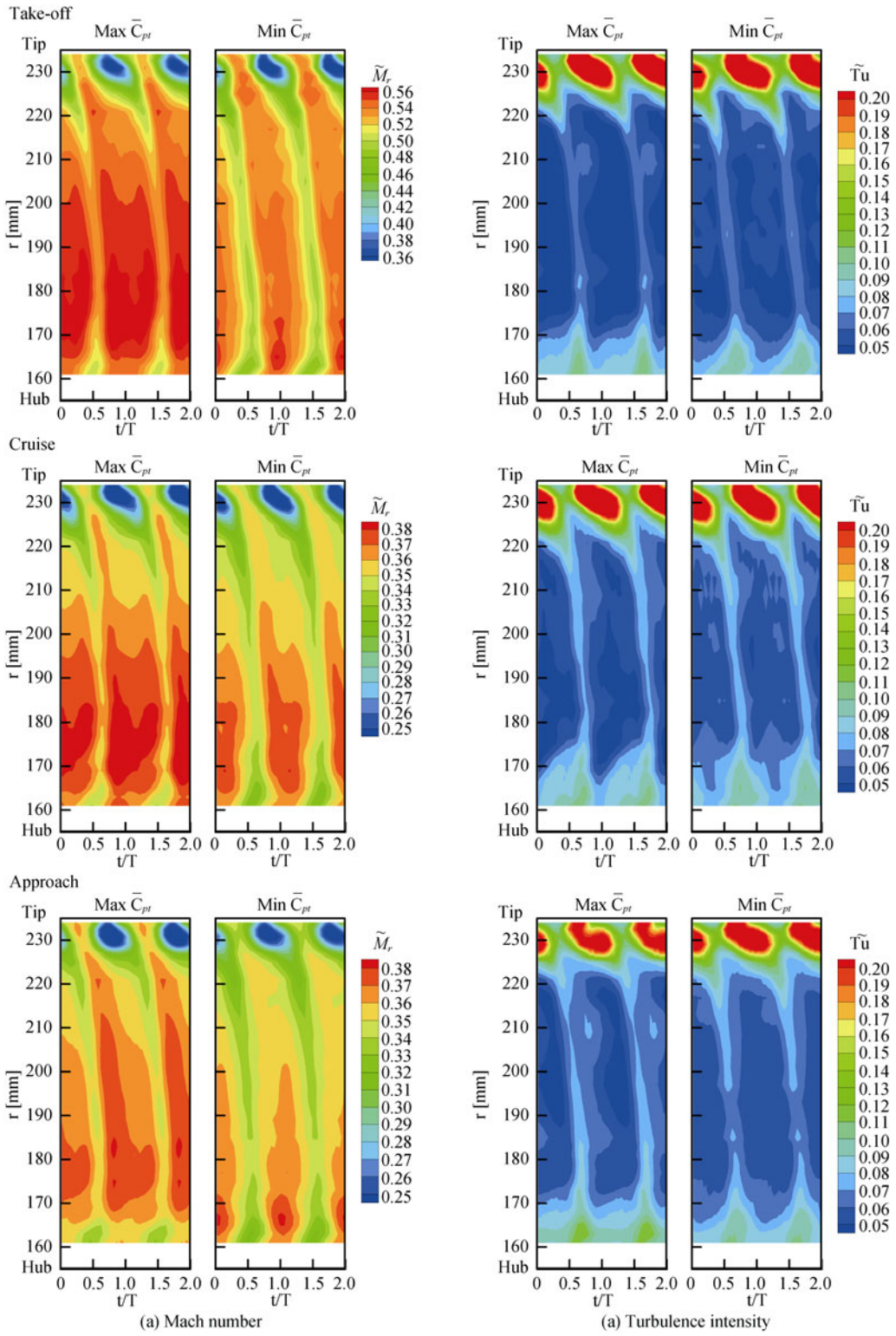

Fig. 6 Contour plots of Mach number and turbulence intensity for three operating conditions; from top to bottom: take-off, cruise, approach; two probe positions are shown for each condition.

teraction between the stator secondary flows and the tip leakage flow. At the same time, at the hub, the effect of the stator secondary flows is modifying the hub secondary vortex of the rotor. This is evident for all the operating points, the hub secondary vortex presents a larger velocity defect for the circumferential position at mini-

mum $\overline{C}_{pt}$ than for maximum $\overline{C}_{pt}$. From 15% to 80% of the blade span, the effect of the different circumferential positions may be observed for all the operating points in the thickening of the wake width and in a slight reduction of the average Mach number.

The turbulence intensity plots (Fig. 6b) provide more information on the flow structures and loss generating mechanisms. As observed by many other studies on turbine rigs, the decrease of the Reynolds number leads to higher turbulence intensity (e.g. [6, 28]). This finding may be observed also in the present results comparing the different Reynolds numbers at equivalent position of the probe (maximum or minimum $\overline{C}_{pt}$). In the present experiments, the average turbulence intensity measured from 15% to 80% of the blade span increases from 5.5% at takeoff to 6.5% at cruise while the inlet turbulence was keeps constant. Similarly the variation of the inlet flow angle (approach) leads to an increase of the turbulence intensity. Furthermore the turbulence intensity is always higher in the circumferential positions at minimum $\overline{C}_{pt}$. This position corresponds to the stator wake which is seen from the probe at a fixed circumferential position as a larger $\widetilde{Tu}$. The rotor wake may be identified, as a local narrow increase of $\widetilde{Tu}$, the maximum of which is slightly shifted towards the pressure side of the wake width. Such aspect is coherent with what found by Arndt [6]. The generation of turbulence on the pressure side shear layer of the wake is not a negligible contribution to the loss generated downstream of a turbine. In this position, in fact, the shear layer is steeper than it on the suction side and it may generate a stronger mixing between the high velocity core flow and the low momentum wake. On the other hand, large values of $\widetilde{Tu}$ are measured in the rotor core flow (between the two wakes shown in the diagrams) both on suction side and pressure side according to the probe position as effect of the stator wake that is chopped and stretched by the rotor potential field. Furthermore, according to the flow condition, the traces of the stator wake are stretched differently from 15% span to 80% span.

The largest turbulence fluctuations occur in the endwall regions. Particularly, in the tip region, $\widetilde{Tu}$ is always larger than 20% and this value is not affected by the variation of the Reynolds number. Whereas the penetration in the midspan region of the area at high $\widetilde{Tu}$ due to the tip leakage vortex slightly changes between take-off and cruise. At low Reynolds numbers, this area is about 25% of the blade span against 20% for high Re.

At the hub, the maximum value of $\widetilde{Tu}$ is 14%, which is a typical value for secondary flows (see for example Porreca et al. [9]). A particular interaction between secondary flows of stator and rotor may be identified in the three flow conditions. At maximum $\overline{C}_{pt}$ the velocity defect is very small, as previously observed, while turbulent fluctuations are large for the whole blade passing period. Whereas, at minimum $\overline{C}_{pt}$ there is a large velocity defect but a smaller extension of the area at high turbulence. Such phenomena may be justified just by a positive effect of the stator hub secondary flow on the momentum deficit of the rotor hub secondary flow.

Conclusions

A post processing procedure for the determination of the turbulence intensity in a turbine test rig by means of a fast response aerodynamic pressure probe has been presented in the paper. Parts of the procedure, the identification of the periodic unsteadiness related to the rotor and the filtering of other sources of deterministic unsteadiness, may also be applied to other measurement techniques in order to distinguish stochastic fluctuations from deterministic fluctuations.

By means of this procedure, the development of the unsteady flow downstream of a LP turbine rotor has been reported in the paper. The 1 and 1/2 stage is representative for a modern LP turbine. Thus the data set provided may be applied for computational code validation. Furthermore, the time resolved measurements have been used to discuss the features that characterize the unsteady flow field for different Reynolds numbers and inlet flow angles.

The largest fluctuations of velocity occur in the tip region, where a large tip leakage vortex is developing for the unshrouded rotor. Secondary flows, at hub and tip, are strongly modulated by the stator structures. While the portion of the blade span not influenced by secondary flows presents lower values of the turbulence intensity, where the largest fluctuations are generated by the shear layers of the rotor wakes. The decrease of the Reynolds number increases the turbulence generation and modifies the structure of the flow.

The methodology proposed allows a detailed study of the flow downstream of the LP turbine confirming the possibility of the use of FRAPP for the analysis of turbulent fluctuations in complex turbine rigs. This procedure will be a starting point for the determination of the turbulence generation in a counter rotating two spool turbine rig. In such a facility, the deterministic unsteadiness of the two rotors has to be filtered in order to measure the stochastic fluctuations of velocity.

Acknowledgement

Paolo Gaetani and Giacomo Persico from Politecnico di Milano are gratefully acknowledged for their support and manufacturing and calibration of the FRAPP. The authors would like to thank H.P. Pirker and E. Göttlich

for operating the compressor station. Thanks to M.Moser for his support. Furthermore, the EU project VITAL, contract no. AIP4-CT-2004-012271, is acknowledged in which the stage was designed, manufactured and operated.

References

[1] Binder, A., Förster, W., Kruse, H., and Rogge, H.: Experimental Investigation into the Effect of Wakes on the Unsteady Turbine Rotor Flow, ASME Journal of Engineering for Gas Turbines and Power, Vol. 107, No. 2, pp. 458–465, (1985).

[2] Hodson, H. P.: Measurements of Wake- Generated Unsteadiness in the Rotor Passages of Axial Flow Turbines, ASME Journal of Engineering for Gas Turbines and Power, Vol. 107, No. 2, pp. 467–476, (1985).

[3] Sharma, O. P., Pickett, G. F., and Ni, R. H.: Assessment of Unsteady Flows in Turbines, ASME Journal of Turbomachinery, Vol. 114, January, pp. 79–90, (1992).

[4] Pullan, G.: Secondary Flows and Loss Caused by Blade Row Interaction in a Turbine Stage, ASME Journal of Turbomachinery, Vol. 128, July, pp. 484-491, (2006).

[5] Persico, G., Mora, A., Gaetani, P., and Savini, M.: Unsteady Aerodynamics of a Low Aspect Ratio Turbine Stage: Modeling Issues and Flow Physics, In Proceedings of ASME Turbo Expo 2010, June 14–18, Glasgow, UK, ASME Paper No. GT2010-22927, (2010).

[6] Arndt, N.: Blade Row Interaction in a Multistage Low-Pressure Turbine, ASME Journal of Turbomachinery, Vol. 115, January, pp. 137–146, (1993).

[7] Hodson, H. P., and Howell, R. J.: The Role of Transition in High Lift Low Pressure Turbines for Aero Engines, Progress in Aerospace Science, Vol. 41, No. 6, August, pp. 419–454, (2005).

[8] Zaccaria, M. A., and Lakshminarayana, B.: Unsteady flow field due to nozzle wake interaction with the rotor in an axial flow turbine: Part 1 – rotor passage flow field, ASME Journal of Turbomachinery, Vol. 119, April, pp. 201–213, (1997).

[9] Porreca, L., Hollenstein, M., Kalfas, A. I., and Abhari, R. S.: Turbulence Measurements and Analysis in a Multistage Axial Turbine, Journal of Propulsion and Power, Vol. 23, No. 1, pp. 227–234, (2007).

[10] Persico, G., Gaetani, P., and Paradiso, B.: Estimation of Turbulence by Single-Sensor Pressure Probes, In XIX Biannual Symposium on Measuring Techniques in Turbomachinery, Rhode-Saint-Genese, Belgium (2008).

[11] Paradiso, B., Persico, G., Gaetani, P., Schennach, O., Pecnik, R., and Woisetschläger, J.: Blade Row Interaction in a One and a Half Stage Transonic Turbine Focusing on Three Dimensional Effects-Part 1: Stator-Rotor Interaction, In Proceedings of ASME Turbo Expo 2008, June 9-13, Berlin, Germany, ASME Paper No. GT2008-50291, (2008).

[12] Camp, T. R., and Shin, H.-W.: Turbulence Intensity and Length Scale Measurements in Multistage Compressors, ASME Journal of Turbomachinery, Vol. 117, January, pp. 38–46, (1995).

[13] Oro, J. M. F., Dıaz, K. M. A., Morros, C. S., and Marigorta, E. B.: On the Structure of Turbulence in a Low-Speed Axial Fan with Inlet Guide Vanes, Experimental Thermal and Fluid Science, Vol. 32, pp. 316–331, (2007).

[14] Moser, M., Kahl, G., Kulhanek, G., and Heitmeir, F.: Construction of a Subsonic Test Turbine Facility for Experimental Investigations of Sound Generation and Propagation for Low Pressure Turbines, In ISABE conference Beijing, Paper No. ISABE-2007-1366, (2007).

[15] Hourmouziadis, J.: Aerodynamic Design of Low Pressure Turbines, Agard lecture series, 167, Toronto, Canada, (1989).

[16] Persico, G., Gaetani, P., and Guardone, A.: Design and Analysis of New Concept Fast-Response Pressure Probes, Meas. Sci. Technol., Vol. 16, pp. 1741–1750, (2005).

[17] Enghardt, L., Tapken, U., Neise, W., Kennepohl, F., and Heinig, K.: Turbine Blade/Vane Interaction Noise: Acoustic Mode Analysis Using in-Duct Sensor Rakes, In Proceedings of the Seventh AIAA/CEAS-Aeroacoustics Conference, Maastricht, The Netherlands, 28-30 May, Paper No. 2001–2153, (2001).

[18] Gaetani, P., Persico, G., Dossena, V., and Osnaghi, C.: Investigation of the Flow Field in a High-Pressure Turbine Stage for Two Stator-Rotor Axial Gaps-Part 2: Unsteady Flow Field, ASME Journal of Turbomachinery, Vol. 129, July, pp. 580–590, (2007).

[19] Hussain, A., and Reynolds, W.: The Mechanics of an Organized Wave in Turbulent Shear Flow, Journal of Fluid Mechanics, Vol. 41, pp. 241–258, (1970).

[20] Suder, K. L., Hathaway, M. D., Okiishi, T. H., Strazisar, A. J., and Adamczyk, J. J.: Measurements of the Unsteady Flow Field Within the Stator Row of a Transonic Axial-Flow Fan. Part I Measurement and Analysis Technique, NASA technical memorandum 88945, (1987),.

[21] Wallace, J. D., and Davis, M. R. D.: Turbulence Measurements with a Calibrated Pitot Mounted Pressure Transducer, In 13th Symposium on Measuring Techniques in Turbomachinery, Zürich, (1996).

[22] Persico, G., Dossena, V., and Gaetani, P.: On the Capability of Fast Response Total Pressure Probes toMeasure Turbulence Kinetic Energy, In XX Biannual Symposium on Measuring Techniques in Turbomachinery, Milano, It-

aly, (2010).

[23] Bindon, J. P.: The Measurement and Formation of Tip Leakage Loss, ASME Journal of Turbomachinery, Vol. 111, July, pp. 257–263, (1989).

[24] Arts, T., (ed.): Turbine Blade Tip Design and Tip Clearance Treatment, VKI Lecture Series, LS 2004-02, Brussels, (2004).

[25] Miller, R. J., Moss, R. W., Ainsworth, R. W., and Harvey, N. W.: The Development of Turbine Exit Flow in a Swan-Necked Inter-Stage Diffuser, In Proceedings of ASME Turbo Expo 2003, June 16-19, Atlanta, Georgia, USA, ASME Paper No. GT-2003-38174, (2003).

[26] Binder, A., Schröder, T., and Hourmouziadis, J.: Turbulence Measurements in a Multistage Low-Pressure Turbine, ASME Journal of Turbomachinery, Vol. 111, No. 2, April, pp. 153–161, (1989).

[27] Lengani, D., Paradiso, B., Marn, A., and Göttlich, E.: Identification of Spinning Mode in the Unsteady Flow Field of a LP Turbine, In Proceedings of ASME Turbo Expo 2011, June 6-10, Vancouver, Canada, ASME Paper No. GT2011-46226, (2011).

[28] Canepa, E., Lengani, D., Ubaldi, M., and Zunino, P.: An Experimental Investigation of the Reynolds Number Variation Effect on Rotor-Stator Interaction in an Axial Two-Stage Pressure Turbine, In Proceedings of the 8th ISAIF, July, Lyon, France, 2007, ISAIF8-091, (2007).